Supplemental Material

Solvent-dependent molecular structure of ionic species directly measured by ultrafast X-ray solution scattering

Kyung Hwan Kim, Jae Hyuk Lee, Joonghan Kim, Shunsuke Nozawa, Tokushi Sato, Ayana Tomita, Kouhei Ichiyanagi, Hosung Ki, Jeongho Kim, Shin-ichi Adachi, Hyotcherl Ihee

Supplementary Methods

Experimental setup

The time-resolved X-ray solution scattering experiment was conducted by using the laser pump–X-ray probe scheme at the beamline NW14 at KEK. Second harmonic generation of the output pulses from an amplified Ti:Sapphire laser system provided femtosecond pulses at 400 nm centre wavelength at a repetition rate of 1 kHz. The frequency-doubled laser pulses were stretched to ~2 ps by passing through fused silica rods to avoid the multiphoton excitation of the sample. The laser beam was focused by a lens to a spot with 300 μm diameter, where the laser beam overlaps with the X-ray beam with the crossing angle of 10°. At the sample, the pulse energy was 240 μJ, yielding a fluence of ~2.6 mJ/mm^2. The laser pulses were synchronized with X-ray pulses from the synchrotron by an active feedback control loop that adjusts the laser oscillator cavity length, and the relative time delay between the laser and x-ray pulses was controlled electronically. The time-delayed X-ray pulses were selected by using a synchronized mechanical chopper. A multilayer optic coated with depth-graded Ru/C layers (d = 40 Å, NTT Advanced Technology, Japan) produced a Gaussian-type X-ray spectrum with a ~5 % energy bandwidth at the centre wavelength of 0.71 Å from the undulator spectrum. The 100 ps-long (FWHM) X-ray pulses with 3×10^8 photons per pulse were focused into a 260×290 μm^2 spot at the sample. The scattering patterns were collected with an area detector (MarCCD165, Mar USA) with a sample-to-detector distance of 40 mm. Three types of I_3^- solutions were prepared by mixing I_2 and KI (from Aldrich, reagent grade) with 1:1 molar ratio in methanol, acetonitrile and water with the concentrations of 10 mM, 3 mM and 1.5 mM, respectively. Since I_3^- ion is formed via equilibrium between (I_2 + I^-) and I_3^-, some of I_2 and I^- may still exist in solution. Those remaining reactants may cause complexity in the analysis of static X-ray scattering but not in the pump-probe scheme used in this work. Since I^- does not absorb at 400 nm and the extinction coefficient of I_2 at 400 nm is smaller than that of I_3^- by a factor of ~100, I_2 and I^- do not undergo photoinduced reactions effectively by 400 nm irradiation. Therefore, the scattering signals from the remaining reactants (I_2 and I^-) are cancelled off by the pump-probe differencing

scheme and do not appear in the difference scattering data. The solution was circulated through a high-pressure sapphire slit nozzle (0.3 mm thickness and ~3 m/s jet speed). Scattering data were collected for three time delays from 100 ps to 1 ns and, for each delay, the reference scattering curve was measured at –3 ns, which represents the unperturbed sample and is subtracted from the data measured at a positive time delay.

Data analysis

Theoretical X-ray scattering intensities are calculated using standard diffuse X-ray scattering formulas. The difference X-ray scattering curve $\Delta S(q,t)_{\text{theory}}$ includes three components, solute-only term, solute-solvent cross term, and solvent-only term:

$$\Delta S(q,t)_{theroy} = \Delta S(q,t)_{solute-only} + \Delta S(q,t)_{solute-solvent} + \Delta S(q,t)_{solvent-only}$$

The solute-only term was calculated using the Debye equation. The solute-solvent cross terms are calculated from the pair distribution functions obtained from MD simulation. The solvent-only term was obtained by a separate solvent-heating experiment where the pure solvent is vibrationally excited by near-infrared light. The solvent-only terms for various solvents are shown in Figure S4, and the cage terms are shown in Figure S5. The relative contributions of the solute-only term, the solvent-only term, and the cage term to the best fit are presented in Figure S6.

Fitting and error analysis

To extract the structure of I_3^- ion from the difference scattering intensity, the maximum likelihood estimation (MLE) with chi-square estimator [1-3] was employed with five variable parameters. The parameters are three bond distances for I_3^- ion (R_1, R_2, and R_3 for the distance between I_1 and I_2, I_2 and I_3, I_1 and I_3, respectively), the bond distance for I_2^- fragment (R_4), and temperature change.

The chi-square (χ^2) is given by the following equation,

$$\chi^2(R_1,\ R_2,\ R_3,\ R_4,\ \Delta T) = \frac{1}{N-p-1}\sum_i \frac{(\Delta S_{theory}(q_i) - \Delta S_{\exp}(q_i))^2}{\sigma_i^2}$$

where N is the total number of q points (which is 1080 for our experimental data), p is the number of fitting parameters (which is 5 without constraint and 4 with constraint), and σ_i is the standard deviation at i^{th} q-point. The likelihood (L) is related to the χ^2 by the following equation,

$$L(R_1,\ R_2,\ R_3,\ R_4,\ \Delta T) \propto \exp(-\chi^2/2)$$

The errors of multiple fitting parameters are determined from this relationship by calculating boundary values of 68.3% of likelihood distribution. The calculation was done by MINUIT software package and the error values are provided by MINOS algorithm in MINUIT.

Since we are using the standard deviation of the measurement when we calculate χ^2, the quality of the fit becomes better if the χ^2 approaches to 1.

I_3^- photodissociation kinetics

The photodissociation kinetics of I_3^- ion in solution has been studied using various time-resolved spectroscopic techniques such as transient absorption and resonance Raman measurements [4-6]. One of the focuses in those studies was the early-time dynamics involving the pathways of two-body dissociation into I_2^- and I fragments and three-body dissociation into I^- and 2I fragments. Possible reaction pathways are summarized in Figure S2. The branching ratio varies with the excitation wavelength. With 266 nm laser excitation, both two-body and three-body dissociation can occur with a certain branching ratio (~8:2). However, with 400 nm laser excitation, it was reported that only two-body dissociation occurs due to the lack of enough energy to break another bond.

The analysis of our own data using three different reaction pathways well matches the results of previous studies [4-6]. If we consider all the reaction channels, the contributions from three-body dissociation and I_2^- formation converge to zero, and only two-body dissociation channel can fit the experimental data (Figure S3).

Computational details of DFT calculations

All molecular structures were optimized using density functional theory (DFT) method. Subsequently, harmonic vibrational frequency calculations were performed using the optimized molecular structures. We used the recently-developed ωB97XD functional [7] as DFT exchange-

correlation functional. To treat the scalar relativistic effect of iodine, we used aug-cc-pVDZ-PP small-core relativistic effective core potential (RECP) [8]. For other atoms (O and H), 6-31++G(d) basis sets were used. We also used the integral-equation-formalism polarizable continuum model (IEFPCM) method [9] to describe solvent effect implicitly. The molecular structure of I_3^- was optimized with a total of 34 surrounding explicit water molecules to form the first solvation shell around I_3^- ion. We used the natural population analysis (NPA) for characterizing atomic charge. All DFT calculations were performed using the Gaussian09 program [10]. The optimized structure of I_3^- ion has a broken symmetry (asymmetric, bent). The elongated iodine atom has a higher negative charge and thus strongly interacts with the adjacent hydrogen atoms of water molecules through hydrogen-bonding interaction. Due to this interaction, the asymmetric and bent ion in the solvation shell is more stable than the symmetric and linear ion. To provide the reference for the energy, a single point energy calculation was performed after changing the molecular structure of I_3^- ion to a linear symmetric one while the structural configuration of the 34 solvent molecules were fixed as the optimized on for the asymmetric case.

Supplementary Tables

TABLE S1. Description of fitting parameters

Parameter	Description
R_1	Distance between I_1 and I_2
R_2	Distance between I_2 and I_3
R_3	Distance between I_1 and I_3
R_4	Bond length of I_2^- ion
ΔT	Temperature change

TABLE S2. Summary of the parameters used for each fitting conditions.

	Constraint	Parameters					# of parameters
		R_1	R_2	R_3	R_4	ΔT	
In water	No constraint	o	o	o	o	o	5
	$R_1 = R_2$	o	×	o	o	o	4
	$R_1+R_2 = R_3$	o	o	×	o	o	4
In MeOH	No constraint	o	o	o	o	o	5
	$R_1 = R_2$	o	×	o	o	o	4
	$R_1 + R_2 < R_3$	o	o	×	o	o	4
In MeCN	No constraint	o	o	o	o	o	5
	$R_1 > R_2$	o	×	o	o	o	4
	$R_1 + R_2 < R_3$	o	o	×	o	o	4

Supplementary Figures

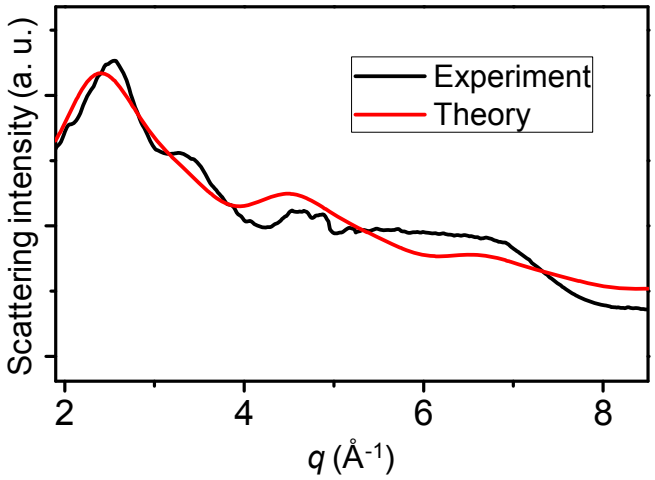

FIG S1. Scattering intensity of I_3^- ion extracted from static wide-angle X-ray solution scattering (black). Scattering patterns from pure solvent and air as well as the dark response of the detector were subtracted from the scattering pattern of the solution sample. The theoretical scattering curve (red) does not match the experimental difference curve due to the unknown background remaining. Therefore, we cannot obtain the exact structure of I_3^- ion within a reasonable error range.

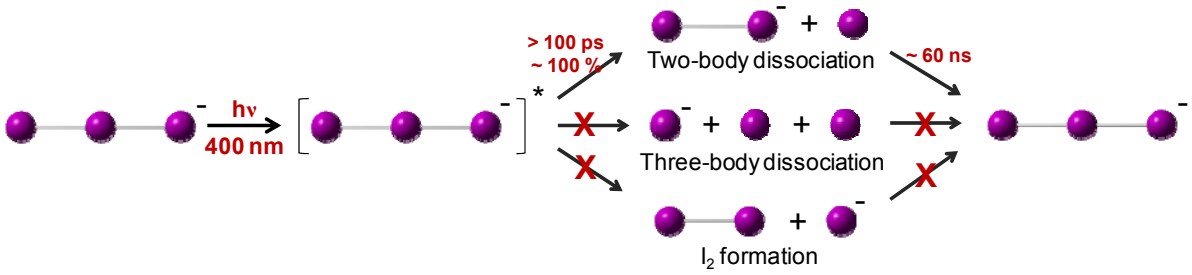

FIG S2. Schematic for candidate reaction channels of I_3^- photodissociation in solution. According to the previous spectroscopic studies and our analysis presented in Figure S3, only two-body dissociation (i.e., I_3^- dissociates into I_2^- and I) occurs by 400 nm laser excitation.

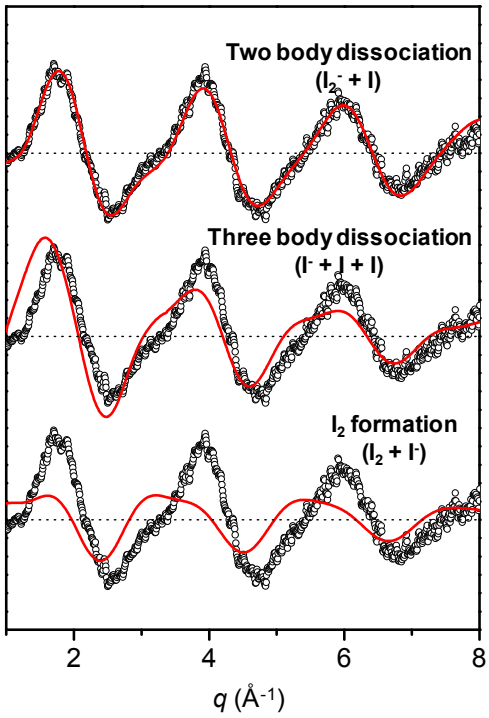

FIG S3. Determination of the reaction pathway of I_3^- photodissociation in solution. Theoretical difference scattering curve (red) for each candidate pathway is overlaid with the experimental difference scattering curve (black). It shows that the two-body dissociation into I_2^- and I is the dominant reaction pathway. If we consider all the reaction pathways together, the contributions from the three-body dissociation and the I_2 formation converge to zero.

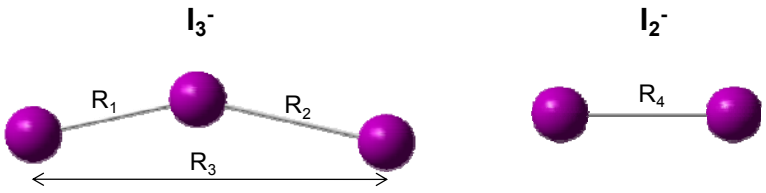

FIG S4. Definition of fitting parameters

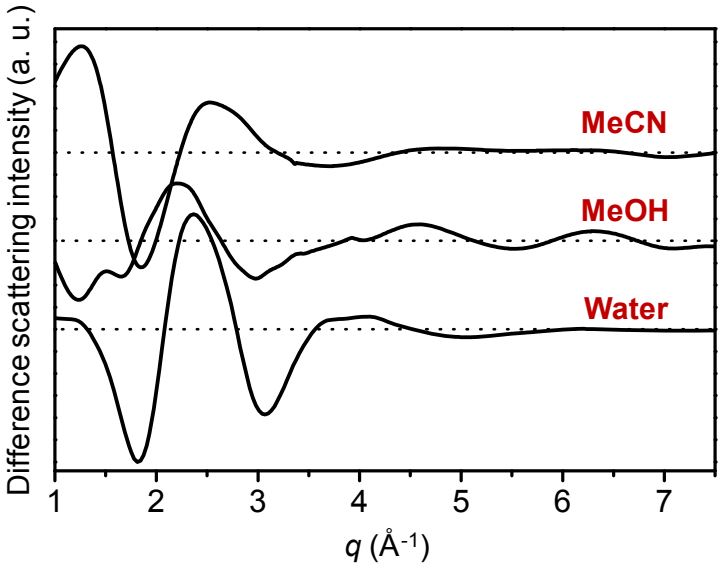

FIG S5. Solvent heating signals (at 100 ps) of water, methanol, and acetonitrile were measured by the separate solvent-heating experiment, of which the detailed procedures are described in our previous publication [11]. These heating signals were used for calculating the temperature change of the I_3^- solutions after photolysis.

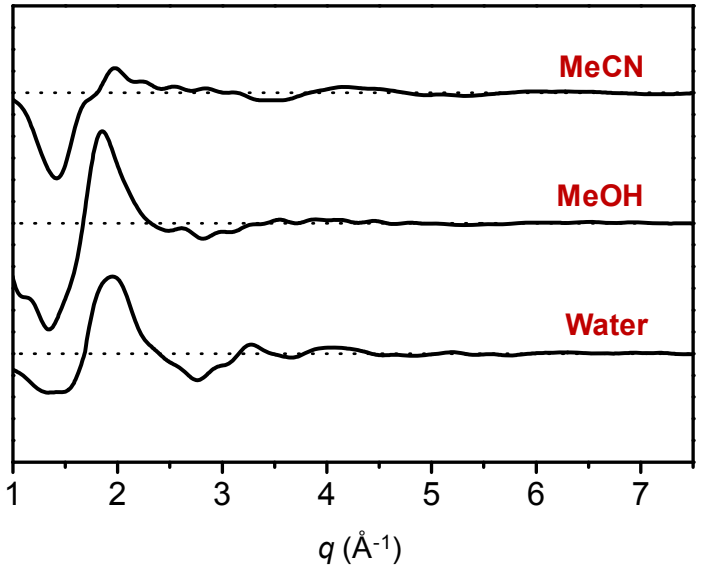

FIG S6. Difference scattering intensities of the solute-solvent cross term (or cage term) were calculated by the MD simulation, of which the detailed procedures are described in one of our previous publications [12-14].

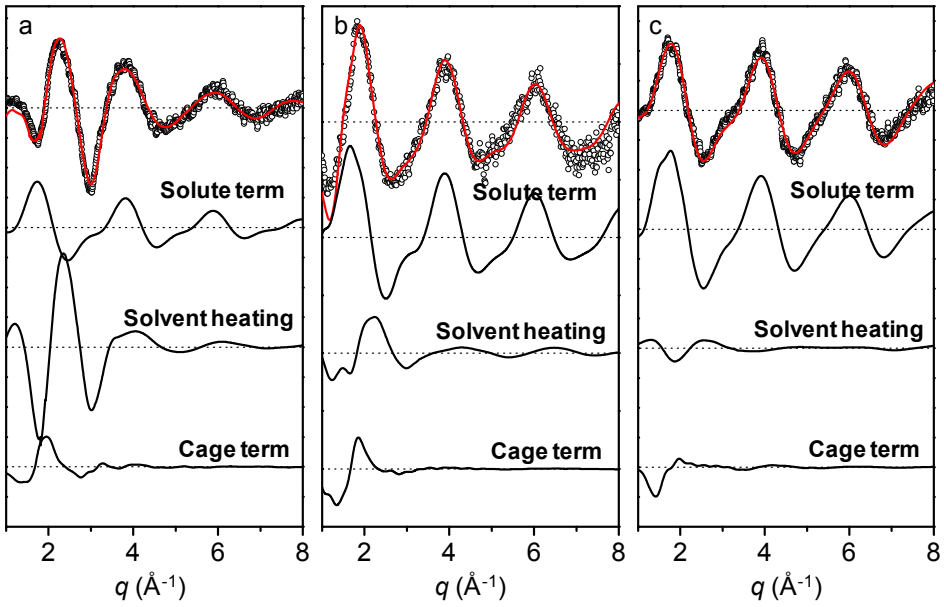

FIG S7. Relative contributions of solute-only term, solvent-only term, and cage term to the best fit in (a) water solution, (b) MeOH solution, and (c) MeCN solution. Experimental (black circle) and theoretical (red) scattering curves) are displayed at the top.

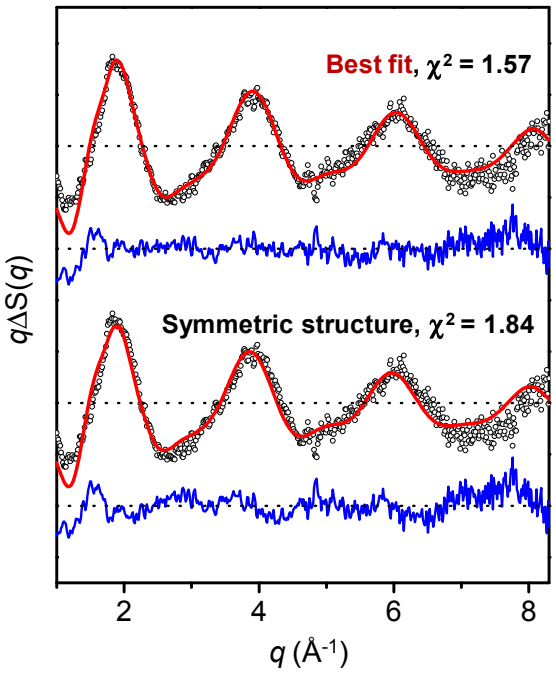

FIG S8. Difference scattering curve from the I_3^- photolysis in methanol solution and its fitting analysis. Experimental (black) and theoretical curves (red) obtained from various candidate structures of I_3^- ion are compared. Residuals (blue) are displayed at the bottom. In methanol, I_3^- ion was found to have an asymmetric and linear structure ($R_1 > R_2$ and $R_1 + R_2 = R_3$). When other structure, for example a symmetric ($R_1 = R_2$) structure, was assumed as a constraint, the agreement between experiment and theory became worse.

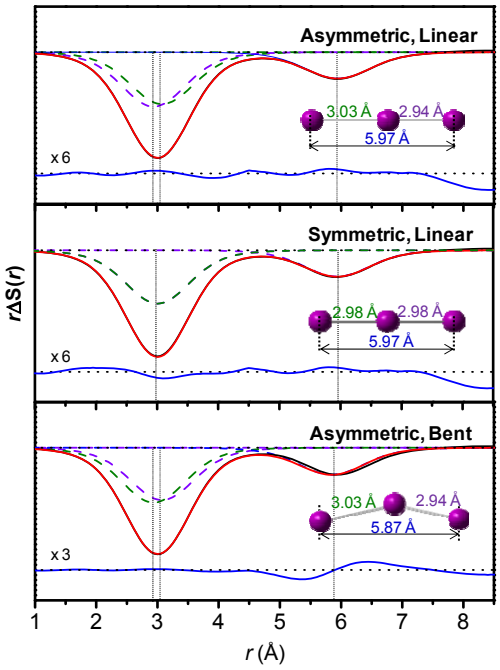

FIG S9. Structure reconstruction of I_3^- ion in methanol solution based on the extracted bond distances. Theoretical curves (red) were generated by a sum of three I-I distances (dashed lines) and compared with the experimental curve. The residuals (blue solid line) are displayed at the bottom. In methanol solution, the theoretical curve calculated from the asymmetric and linear structure gave the best fit to the experimental curve (top panel). When one average distance (2.99 Å) instead of two unequal distances was used, the broad feature in the experimental curve cannot be matched (middle panel). When a bent structure was used, the peak at 5.95 Å is shifted to a smaller value, giving a worse fit to the experimental curve (bottom panel).

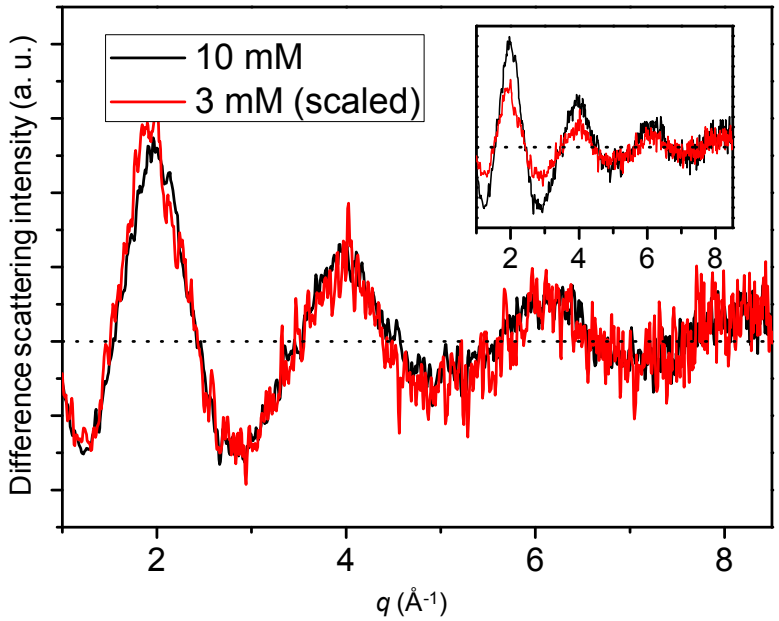

FIG S10. Concentration dependence of the difference scattering curve. The scattering curves measured from the I_3^- ion solutions of 3 mM and 10 mM concentrations have the same shape after scaling, indicating that there is no concentration dependence in this concentration range. Inset shows the original data.

Supplementary References

[1] M. Christensen *et al.*, J. Am. Chem. Soc. **131**, 502 (2009).
[2] K. Haldrup *et al.*, Angew. Chem. Int. Ed. **48**, 4180 (2009).
[3] S. Jun, J. H. Lee, J. Kim, K. H. Kim, Q. Kong, T. K. Kim, M. Lo Russo, M. Wulff, and H. Ihee, Phys. Chem. Chem. Phys. **12**, 11536 (2010).
[4] U. Banin and S. Ruhman, J. Chem. Phys. **98**, 4391 (1993).
[5] T. Kuhne, R. Kuster, and P. Vohringer, Chem. Phys. **233**, 161 (1998).
[6] L. Zhu, K. Takahashi, M. Saeki, T. Tsukuda, and T. Nagata, Chem. Phys. Lett. **350**, 233 (2001).
[7] J.-D. Chai and M. Head-Gordon, Phys. Chem. Chem. Phys. **10**, 6615 (2008).
[8] K. A. Peterson, B. C. Shepler, D. Figgen, and H. Stoll, J. Phys. Chem. A **110**, 13877 (2006).
[9] E. Cances, B. Mennucci, and J. Tomasi, J. Chem. Phys. **107**, 3032 (1997).
[10] M. J. Frisch *et al.*, Gaussian 09, Gaussian, Inc., 2009.
[11] M. Cammarata *et al.*, J. Chem. Phys. **124**, 124504 (2006).
[12] H. Ihee, M. Lorenc, T. K. Kim, Q. Y. Kong, M. Cammarata, J. H. Lee, S. Bratos, and M. Wulff, Science **309**, 1223 (2005).
[13] H. Ihee, Acc. Chem. Res. **42**, 356 (2009).
[14] T. K. Kim, J. H. Lee, M. Wulff, Q. Y. Kong, and H. Ihee, ChemPhysChem **10**, 1958 (2009).